



DEPARTMENT OF BIOSYSTEMS SCIENCE & ENGINEERING



---

SEMESTER RESEARCH PROJECT:

---

# Connectivity Inference for Small-Scale Neuronal Networks

Impact of Firing Behaviour & Network Topology of  
adaptive-Exponential Integrate-and-Fire Neurons

---

*Author:*  
Gordon J. Köhn

*Working Period:*  
Feb. 21 - Aug. 26

*Supervisor:*  
TaeHoon Kim

*Duration:*  
12 weeks

A report submitted for the degree of

*MSc Biotechnologie*

August 19, 2022



## Abstract

In the pursuit to comprehend the enigmatic nature of our brain, understanding operational principles of neural circuits is the main goal. The defining characteristic of any circuit is its connectivity. Yet, investigating the physical neuron to neuron connections in the living brain on a large scale is presently still infeasible. Thus, other methods to learn about the connectivity of neuronal circuits are being explored, as for instance via the neural activity. The dawn of high-density, multi-electrode implants gives hope to record large-scale neuronal activity on the single neuron level in next decades.

Given neuronal activity recordings, the functional connectivity of a network may be inferred from statistical correlation. The term functional connectivity separates the connectivity found by correlation from the physical, called structural connectivity. It may already contain the operational principles of our brain we seek to find.

Here, we evaluate the performance of a widely used functional connectivity inference method by English et al. [2017] on small-scale networks. We generate neural activity in silico on a known random network structure, to then evaluate the performance of the algorithm against it.

The model used to simulate neurons is the prominent adaptive-Exponential Integrate-and-Fire (aEIF) model by Brette et al. [2007], allowing to capture the fundamental exponential and adapting behaviour of the action potential.

The performance of the connectivity inference algorithm is evaluated at the extrema of synchrony of sensible network activity. Therefore an extensive parametric study in the adaptation and conductance space of the used neuron model was conducted, successfully identifying regimes of a- and synchronous activity.

Particular cases of very synchronous network activity lead to a poor performance of the inference algorithm, yet this study fails to make quantitative statements aimed for.

Further, an attempt to explore network activity and performance of the algorithm at more neuro-physiological network topologies, namely scale-free networks is presented.

**Keywords:** Neuron Simulations, Functional Connectivity Inference, adaptive-Exponential Integrate-and-Fire Model, Network Synchrony, Network Topology

# Contents

<b>Abstract</b>	<b>iii</b>
<b>1 Introduction</b>	<b>1</b>
1.1 Background . . . . .	2
1.1.1 Neuron Model: adaptive-Exponential Integrate-and-Fire . . . . .	2
1.1.2 Connectivity Inference: cross-correlation . . . . .	3
<b>2 Network Setup</b>	<b>5</b>
2.1 Conductance & Adaptation Behaviour . . . . .	5
2.1.1 Conductance . . . . .	7
2.1.2 Adaptation . . . . .	8
2.1.3 Extrema example network activities . . . . .	11
<b>3 Impact of Synchrony on Functional Connectivity Inference</b>	<b>13</b>
<b>4 Impact of Topology</b>	<b>17</b>
4.1 Scale-Free Networks . . . . .	17
4.2 Proof-of-Concept Simulations . . . . .	18
4.3 Inhibitory Neurons as Hub Neurons . . . . .	20
<b>5 Discussion &amp; Conclusion</b>	<b>21</b>
<b>Acknowledgements &amp; Declaration of Work</b>	<b>22</b>
<b>Bibliography</b>	<b>23</b>
<b>Appendices</b>	<b>26</b>
<b>Appendix A Full Results of Synchrony - Connectivity Inference</b>	<b>26</b>
<b>Appendix B Source Code</b>	<b>30</b>

# 1 Introduction

We live in an age where the tools and understanding exist to manipulate the human body at the most fundamental level, its genome. Yet, the organ defining our human nature, our brain, and its enigmatic way of information processing are a black box still to be opened fully.

The knowledge we have already acquired about its basic unit, the neuron, and its information processing, have deeply inspired our current way of silicon-based computing. Its early descendent *Machine Learning* and now the dawn of *Neuromorphic Computing* are already impacting our everyday. [Frady and Sommer, 2019]

Breaking the code of the brain's information processing, has been on peoples minds since 1960 with the dawn of personal computers. With the rise of the personal computers, fictional literature picked up the narrative of 'cyborgs', or in today's terminology the 'brain-computer-interface'.<sup>1</sup>

In the current day, international brain science programs, such as the BRAIN Initiative [Insel et al., 2013, Martin and Chun, 2016], and commercial companies, as Neuralink, are working towards visions like this and fundamental neuroscience research questions. Their common goal is to understand the *operational principles of neural circuits*.

Despite advances in learning about how information is represented in the brain through correlation or decoding analyses with relevant sensory, motor, or cognitive signals, the circuit mechanisms that encode or transform information are still missing. 'Knowing the wiring diagram of neuronal circuits is critical to explain how such representations are produced, predicting how the network would behave in a novel situation [...]'. [Magrans de Abril et al., 2018]

As it is currently infeasible to identify the connections of neurons in the living brain on a large scale, alternative ways have to be found to get the connectivity of neuronal networks. The research field of *connectivity inference from neural recording data* addresses this need. The rapidly growing availability of neural recordings through the development of high-density, multi-electrode assays and even implants gives hope to record the needed large-scale neuronal activity on the single neuron level in next decades to reveal the operational principles of the brain (e.g. Multi-electrode-arrays Müller et al. [2015], Neuralink Musk [2019]).

The aim of this study is to evaluate the performance of a prominent connectivity inference algorithm, by English et al. [2017]. This is done by generating neuronal activity in-silico using the well established aEIF neuron model, by Brette et al. [2007]. The main question attempted to answer is: Does the co-activity of neurons (i.e. synchronous or asynchronous firing) influence the performance of the inference?

This report is structured as follows: The remainder of this Section 1 will provide the main principles of the aEIF neuron model and the connectivity inference method used in this study. Section 2 establishes the physical network setup and explores the parametric conductance and adaptation space of the aEIF model to identify regimes of a- and synchronous activity of networks. Section 3 then investigated the impact of synchrony on the performance of the functional connectivity inference, followed in Section 4 by the early attempt to extend that study to different network topologies, namely scale-free networks. A conclusion and outlook is provided Section 5.

---

<sup>1</sup>See Google Ngrams for Cyborgs, Brain-Computer-Interface

## 1.1 Background

The following is intended as a focused introduction to neuron models and connectivity inference - familiar readers may skip.

### 1.1.1 Neuron Model: adaptive-Exponential Integrate-and-Fire

In the pursuit of understanding the emerging function of neurons working together in a network, a promising approach is to simulate neurons in-silico with just enough physiological complexity to capture the spark that makes neuronal networks so highly effective and adaptive computational machines. Such simulations of neurons seek out to describe the key effects governing the action potential, often discarding all other biological workings. Detailed neuron models simulating the conductance of membranes such as Hodgkin and Huxley [1952], capture the electrophysiological behavior of neurons in great detail but determining the up to hundred or more parameters to specific neuron types poses a major experimental challenge. [Brette et al., 2007] Hence, simplified phenomenological neuron models of the integrate-and-fire type sacrifice biophysiological exactness, yet capture observed spiking behavior very well with much fewer model parameters. [Brette et al., 2007] Because of this, integrate-and-fire neuron model are the most widely used class of models for analyzing the behavior of neural systems. [Zhou et al., 2020] It describes the membrane potential of a neuron in terms of the synaptic inputs and the injected current that it receives. An action potential (spike) is generated when the membrane potential reaches a threshold, triggering a current or change in conductance to a connected neuron. A particularly successful integrate-and-fire model is the adaptive Exponential Integrate-and-Fire (aEIF) model by Brette et al. [2007]. It successfully reproduces all major electrophysiological neuron classes (e.g. regular spiking, bursting, chattering) by just changing a few parameters of the model. Its name stems from the fact that the model implements an adaptation current, allowing for the adaptation of the neurons' sensitivity, as well as the implementation of the biological mechanism of hyperpolarization via an exponential term in the membrane potential. The model is defined by two differential equations. The first describes the dynamics of the membrane potential, including the voltage dependent activation of sodium channels, given as

$$C \frac{dV}{dt} = \underbrace{-g_L(V - E_L)}_{\text{leak current}} + \overbrace{g_L \Delta_T \exp\left\{\frac{V - V_T}{\Delta_T}\right\}}^{\text{activation of Na-channels}} \underbrace{-w}_{\text{adaption current}} \underbrace{+ I}_{\text{input current}} \quad (1)$$

and the second describes the dynamics of the adaptation variable,  $w$ , governing the sensitivity to activation as

$$\tau_w \frac{dw}{dt} = a(V - E_L) - w. \quad (2)$$

In the above equations  $V$  and  $I$  denote the membrane voltage and input current respectively. The other variables are parameters of the model as:

$C$	membrane capacitance
$g_L$	leak conductance
$E_L$	leak reversal potential
$V_T$	spike threshold
$\Delta_T$	slope factor
$\tau_w$	adaptation time constant
$a$	subthreshold adaptation
$b$	spike-triggered adaptation

The first four parameters are fixed as they are intrinsic to the particular type of neuron. The remaining parameters can be varied to achieve differnt activity patterns from regular,

fast-spiking to bursting. A spike could be generated as follows: The input current,  $I$ , provided by a connected excitatory neuron, leads to an increase in membrane potential,  $V$ . If this increase is sharp enough, to overcome the counter-effects of leak current and adaptation current, the difference between membrane potential and spike threshold,  $(V - V_T)$  will lead to the exponential term becoming dominant, leading to a spike being triggered. In practice, the evolution of the differential equations is stopped once a certain cutoff potential,  $V_{cut}$ , is reached and a spike is noted at that time-point. The adaptation variable  $w$  of the post-synaptic neuron is increased by the spike-triggered adaptation,  $b$ , leading to a lower sensitivity to stimulus. After a set refractory period, the membrane voltage is set to the resting potential,  $E_L$ , continuing the evolution with an altered value of adaptation current,  $w$ . A complete description of the working of the model is found in the original paper of Brette et al. [2007].

### 1.1.2 Connectivity Inference: cross-correlation

The goal of functional connectivity inference in the context of neural recordings is to learn about the connections between neurons from its recorded spiking activity.

The field focuses on the spatial scale at which connections of neurons are within a local area, as well as their projections to other areas. This scale is called the mesoscopic scale and is thought to be of prime importance for identifying the operational principles of neural circuits. [Magrans de Abril et al., 2018]

Further, it is important to distinguish between several types of connectivity. Ideally, it is the *structural connectivity*, the actual anatomic connections, we would like to learn about. This is different from the *functional connectivity* actually obtainable from inference. The difference is that we obtain the functional connectivity from statistical dependence among measurements of neuronal activity and that the detection of functional connectivity does not warrant the existence of anatomical connectivity. An example would be a false positive connection inferred between two neurons that receive common inputs from a third neuron. Magrans de Abril et al. [2018]

Despite this technical distinction, functional connectivity is thought to contain the operational principles of neuronal circuits and is hence worth obtaining. A fundamental problem of the field is how to check the inferred functional connectivity. The common answer is to compare the functional to the structural connectivity despite describing slightly different features of the network.

The methods to compute functional connectivity are numerous. It can be computed by correlation, various other model-free or model-based methods. The discussion of the vast field is not topic of this study. The review by Magrans de Abril et al. [2018] provides an excellent overview of the field.

This study did choose a model-free method, namely cross-correlation. The method computes the cross-correlation between individual neurons to decide whether or not a connection exists. The particular implementation used here is introduced in English et al. [2017]. A description of the method doing it justice goes beyond the scope of this report, yet let it be said that the core element of the method is the cross-correlogram between any two neurons. This plot compares the frequency of spikes of neuron A in time-windows around a spike times of neuron B. If neuron A frequently spikes shortly after neuron B it may indicate a connection from neuron B to A. Examples of cross-correlograms can be found in Figure 10.

This principle begs the question what happens in cases of very synchronous behaviour, i.e. the commonly observed bursting of neuronal networks. Can cross-correlation still resolve connections from neurons firing at once? The theoretical answer to this surely exaggerated question must be no. Synchronous firing cannot reveal network structure as no time-lag between spikes can suggest a directionality of synapses. The more interesting question this

study tries to answer is how strongly the synchrony of realistic network activity actually influences the performance of functional connectivity inference cross-correlation?

## 2 Network Setup

As connectivity inference is a highly computational discipline, requiring large resources, and the goal was to evaluate the performance of the inference algorithm on a closed network (connected within itself), a small network size was required. We thus set out to simulate a very small neuronal network of  $N = 100$  neurons. This small network size does allow to simulate realistic spiking patterns as regular firing, fast firing and bursting, if some network parameters are adjusted. This however means that the demand of physiological realistic network parameters has to be dropped. Yet for the purpose of evaluating the performance of the inference algorithm that is without consequences, as all that matter are realistic spiking activity patterns.

The neurons were mapped on network topologies generated either as a directed random graph or scale-free graph. Random graphs, more precisely Erdős-Rényi graphs, were generated using the algorithm by Gilbert [1959], assigning an edge for all possible edges with a probability of  $p = 0.02$ . Directed scale-free graphs were generated via the algorithm by Bollobás et al., described in Section 4. Self-connections were forbidden, as they are physiological nonsense.

We implement the two main neuron cell types found in the extracellular human brain recordings: regular-spiking (RF) excitatory and fast-spiking (FS) inhibitory. [Peyrache et al., 2012, Goldman et al., 2021] The cell types are defined by their excitation behaviour as well as their spiking patterns. Excitatory neurons do cause an increase in membrane potential on the post-synaptic neuron. Inhibitory neurons do cause a decrease. It has been widely observed that RS neurons are excitatory and FS neurons are inhibitory in overwhelming quantities. [Inawashiro et al., 1999] The remainder of this report will hence refer to the two main cell types with either regular spiking or excitatory / fast-spiking or inhibitory in synonymous usage.

All neuronal networks simulated are composed of 20% inhibitory ( $N_i = 20$ ) and 80% excitatory ( $N_e = 80$ ) neurons following Susin and Destexhe [2021] as a realistic division.

Most network parameters for the aEIF-model were also taken from Susin and Destexhe [2021], see Table 1 or only slightly varied by trial-and-error for realistic spiking activity. For the leak conductance,  $g_l$ , as well as adaptation time constant,  $a$ , and subthreshold adaptation,  $b$ , a parametric search was run, trying to identify the regimes of physical, a-/synchronous spiking behaviour. Further, synaptic delays were kept at  $1.5\text{ ms}$  for all neurons.

Upon initialization membrane potential were uniform randomly set to be within the range of  $-60$  and  $-50\text{ mV}$ . To further cause activity of the network, initial stimulation was provided in the form of each neuron receiving an external drive (noise). This noise was implemented as 100 independent and identically distributed excitatory Poissonian spike trains with a spiking frequency  $\mu_{Ext}=200\text{ Hz}$  for the first 100 ms of the simulation. All simulations were run for  $10\text{ s}$ . To exclude the initialization phase from all further analysis the first  $1\text{ s}$  of network activity is excluded from all consecutive analysis.

All neural networks were constructed using Brian2 simulator. [Perotti et al., 2006] All equations were numerically integrated using Euler Methods and  $dt = 0.1\text{ ms}$  as integration time step.

### 2.1 Conductance & Adaptation Behaviour

This section explains the reasoning and results of the parametric search conducted in the conductance and adaptation space. The goal, as mentioned afore, of this parametric search was to identify *physical* network activity at the extremes of spiking *synchrony*.

symbol	parameter		value			
			used here		by Susin and Destexhe	
			inhib./FS	excit./RS	inhib./FS	excit./RS
$C$	membrane capacitance	[pF]	200	200	150	150
$g_L$	leak conductance	[nS]	0-80	0-80	67	6
$E_L$	leak reversal potential	[mV]	-80	0	-80	0
$V_T$	spike threshold	[mV]	-50	-50	-65	-65
$\Delta_T$	slope factor	[mV]	2.5	2.5	2	2
$T_{ref}$	refractory period	[ms]	5	5	5	5
$\tau_w$	adaptation time constant	[ms]	600	600	500	500
$a$	subthreshold adaptation	[nS]	0	0-85	0	4
$b$	spike-triggered adaptation	[pA]	0	0-85	0	20

Table 1: Parameters of the adaptive Exponential Integrate-and-Fire (aEIF) model by Brette et al. [2007] for excitatory and inhibitory neurons as set by Susin and Destexhe [2021] for regular spiking (RS) and fast spiking (FS) neurons for 'Asynchronous and Irregular (AI) Networks'. Grey cells are varied through the parametric searches identifying a-/synchronous spiking regimes

The attribute physical is here describing prolonged network activity with mean firing rates of the network between 1-20  $Hz$  (or 1-30 see Section 2.1.2) exclusive. It shall be stressed here that many network setups do not result in prolonged activity or have saturated firing ( $f_s = 1/T_{ref} = 1/5\text{ms} = 200\text{Hz}$ ). Trial and error exploration as well as understanding of the neuron model lead to the conclusion that the conductance of excitatory/RS and inhibitory/FS neurons,  $g_e$  and  $g_i$  respectively in this network setup were the main handles to control the physicality. Exploration of the  $g_e$  and  $g_i$  space, to identify physical candidate pairs ( $g_e, g_i$ ) was hence set out as *Stage 1* of the parametric study.

Upon identified candidates of physical leak conductances we proceed to explore network synchrony. Therefore we vary both adaptation variables  $a_e$  and  $b_e$ . The sub-threshold adaptation,  $a$ , and spike-triggered adaptation,  $b$ , strike as great handles of network synchrony. As these both variables are zero for inhibitory/FS,  $a$  and  $b$  henceforth denote the adaption variable of excitatory/RS neurons, i.e. dropping subscripts.

In order to identify the two desired regimes of activity, namely synchronous and asynchronous, we shall here more closely define what is meant with this. Qualitatively, network activity is here refereed to as synchronous if most neurons belong to groups of neurons that tend to fire at the same times. As a quantitative measure of this behaviour we defined an asynchronous network activity as by having a mean pairwise correlation of  $\bar{\rho}_{corr} < 0.1$  and a coefficient of variation of  $c_v = \frac{\sigma}{\mu} > 1$ . The mean correlation computed is the mean of all  $N \times N$  pairwise Pearson's correlation coefficients between all combinations of  $N$  binned ( $5\text{ms}$ ) spike trains. The requirement of the coefficient of variation was introduced to ensure irregular network activity, that is thought to benefit later connectivity inference as it quantifies the extent of variability in relation to the mean of the population.

Both stages of this parametric search were conducted using a random network topology - randomly generated for each simulation run. Each set of parameters tested was investigated with three independent simulations, i.e. replica. This was done to counter the large statistical variation in mean network firing rates,  $\bar{f}$ , as well as indicators of synchrony ( $c_v, \bar{\rho}_{corr}$ ). One source of variation is the random generation of topology. Variations in topology for neuronal networks of this small size can already have a large effect on its overall activity. The second source of variation is due to the statistical initial external drive.

All network activities presented in the remainder of this section have been checked to be active beyond the initial phase of stimulation, first  $1\text{s}$  of simulation time, but may go

dormant within the 10 s of total simulation time.

This study does not claim having found the absolute extreme of synchrony of this network setup, merely a local optima.

### 2.1.1 Conductance

In order to conduct this parametric study it was necessary to fix the adaptation variables a priori to a sensible value  $(a, b) = (1 \text{ nS}, 5 \text{ pA})$ , based on Susin and Destexhe [2021] for 'Asynchronous and Irregular Networks'. With those adaptation values the leak conductance space was explored in the order of magnitude present in current literature. [Susin and Destexhe, 2021, Destexhe, 2009] Simulations for leak conductance, hereafter referred to as conductance, were run for all combinations of values for excitatory and inhibitory conductance sets  $G_e = [0, 5, \dots, 95, 100] \text{ nS}$  and  $G_i = [0, 5, \dots, 95, 100] \text{ nS}$ , i.e. the conductance space  $C_s = G_e \times G_i$ . A total of 441 simulations with three replicas each, i.e. 1323 simulations were run. All variables of analysis are averaged for the replica, henceforth referred to as replica values or with the subscript  $r$ .

Figure 1 shows the conductance space with respect to the replica mean firing frequency. No saturation of the network is observed at this set of adaptation values - all firing rates below 16 Hz. Low excitatory conductance did show activity with low firing rates and dormant networks. This is an expected observation as a certain level of mutual excitation is necessary for network activity to persist. The striking trend visible is that medium values (20-40) nS of excitatory conductance lead to a steep rise of replica mean firing rates, followed by a much shallower decrease. This must indicate the surpassing of spike threshold potential,  $V_T$ . On the inhibitory conductance axis a weak trend towards higher replica mean firing rates can be seen.

These results allow for many possible choices of conductance pairs. Here  $(g_e, g_i) = (40, 80) \text{ nS}$  was picked. These are relatively large values that would result in relatively mono-synaptic triggering of spikes, beneficial to the performance of functional connectivity inference. Further, the choice reflects the typical dominance of inhibitory to excitatory conductance. [Vogels and Abbott, 2005, Destexhe, 2009]

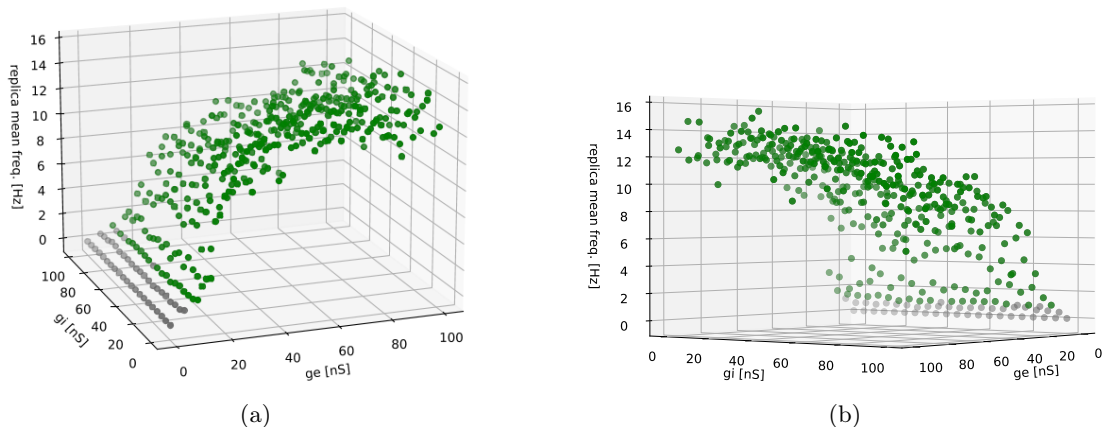


Figure 1: Replica mean firing frequency,  $\bar{f}_r$ , over conductance space  $C_s$  at two different viewing angles a) and b). Green dots are for physical simulations, i.e.  $\bar{f}_r$  of 1-20 Hz.

### 2.1.2 Adaptation

With chosen conductance pair *Stage 2: Adaptation* did explore the adaptation space composed of the cartesian product of the sets  $A = [1, 2, \dots 84, 85] nS$  and  $B = [1, 2, \dots 84, 85] pA$ , i.e  $A_d = A \times B$ . This range of  $a$  and  $b$  was again chosen to explore the order of magnitude found in the literature [Susin and Destexhe, 2021], restricting the upper bound to save computational resources. The adaption space was hence explore with a high resolution, leading to a total of 7396 of conditions, i.e. 22188 simulations for 3 replica.

The replica mean firing frequency,  $\bar{f}_r$ , over this adaptation space is shown in Figure 2. A first striking feature is the absence of many conditions. These conditions did result in one or more dormant networks and have hence been excluded from the subsequent analysis. Secondly, low  $b$  values results in high firing rates, rapidly rising for values below  $b = 20 pA$ . This must be the threshold that single excitation leads to the spike-triggered adaption being large enough to hinder excitation shortly after. If  $b$ , spike-triggered adaption, is hence not above  $\sim 20 pA$  multiple excitation are needed to make a neuron insensitive to further excitation.

On absolute terms, the mean-firing frequency reached very high values of  $160 Hz$ , as expected for condition of no significant spike-triggered adaptation.

The conditions of particular interest, that are asynchronous conditions are found in a layer between  $\sim 22 - 40 Hz$ . This unfortunately is outside of the prior set bounds of physical conditions. Hence, we have to relax the conditions of physicality to  $30 Hz$ , which is still very reasonable with the literature and far below the saturation frequency. The intersection of asynchronous and relaxed physical conditions is interestingly found along an offset diagonal in adaptation space at  $\sim 30 Hz$ .

The distribution of active network conditions becomes visible in Figure 3a. It clearly shows a linear trend that of active network below the trend-line with a slope of less then 1 for  $x = a$  and  $y = b$ . This picture may be explained by recalling the oversimplified functions of  $a$  and  $b$ :  $a$  - subthreshold adaptation: high  $b$  means quicker adaptation decay;  $b$  - spike triggered adaptation: strength of adaptation upon spike. One could hypothesize that,  $a$  has to cause a quick enough decay of adaptation weight,  $w$ , for a certain level of  $b$ , so that the network doesn't fall dormant due to prolonged periods of very high weights  $w$ .

Figure 3b does highlight the distribution of asynchronous simulations of the adaptation space. Unfortunately, no hot-spots sought out for can be spotted, under the strict asynchronous criteria set out earlier. Nevertheless, no asynchronous simulations were found below  $b \sim 13$ , apparently the minimum of spike-triggered adaptation needed for asynchronous spiking.

A closer look at the raw averaged mean pairwise correlation,  $\bar{\rho}_r$ , and coefficient of variation values,  $c_v$ , is shown in Figure 4. Two modes of simulations seem to exist. One mode has high correlation,  $\bar{\rho}_r \sim 0.25$ , and low  $c_v \sim 0.25$  and the other has the reverse at  $\bar{\rho}_r \sim 0.15$  and  $c_v \sim 1.75$ , judging by eye. So there is a rather step like shift from very synchronous, regular to more asynchronous irregular network activity.

As in the binary analysis (is asynchronous + physical or not) so far, no clear candidate or hot-spot of condition(s) has emerged, a more granular search for trends was needed. Therefore, both axis of synchrony were inspected over the adaptation space, see Figure 5. Figure 5a does explain why no asynchronous conditions were previously found in the low  $b$  space. There appears to be a steep rise in coefficient of variation. A less pronounced but still clearly visible sharp change in visible for low  $b$  in Figure 5b, where the correlation falls of for higher  $b$ . The region around  $(a, b) = (\sim 25 nS, \sim 20 pA)$  has both high coefficients of variation and low correlation values, and is hence a favourable region.

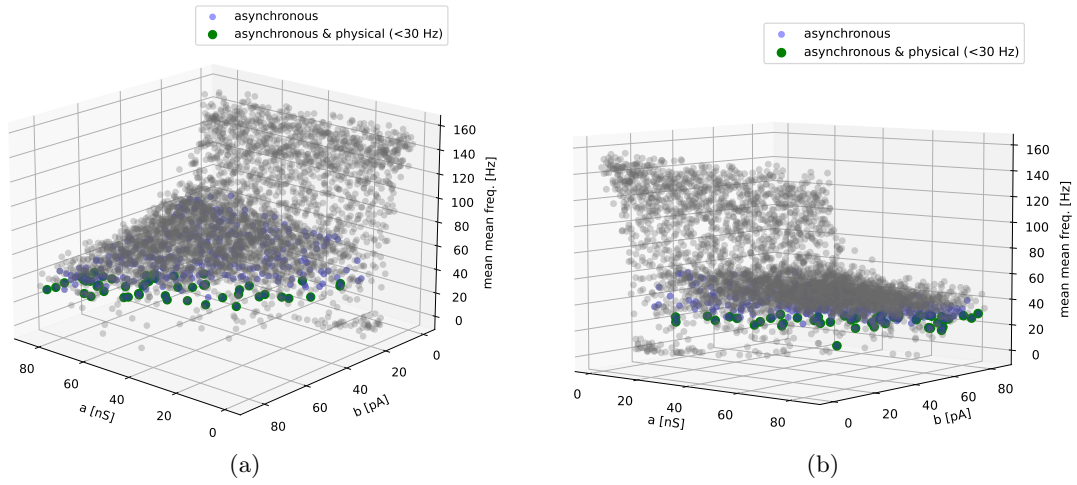


Figure 2: Replica mean firing frequency over the adaptation space from two different perspectives a) and b). A dot represents the average value over the three replicas for that  $(a, b)$  condition. Asynchronous, as defined in Section 2.1 and the intersection with physical conditions are indicated. Note the physical criteria have been extended to 1-30 Hz. Dormant network conditions not shown.

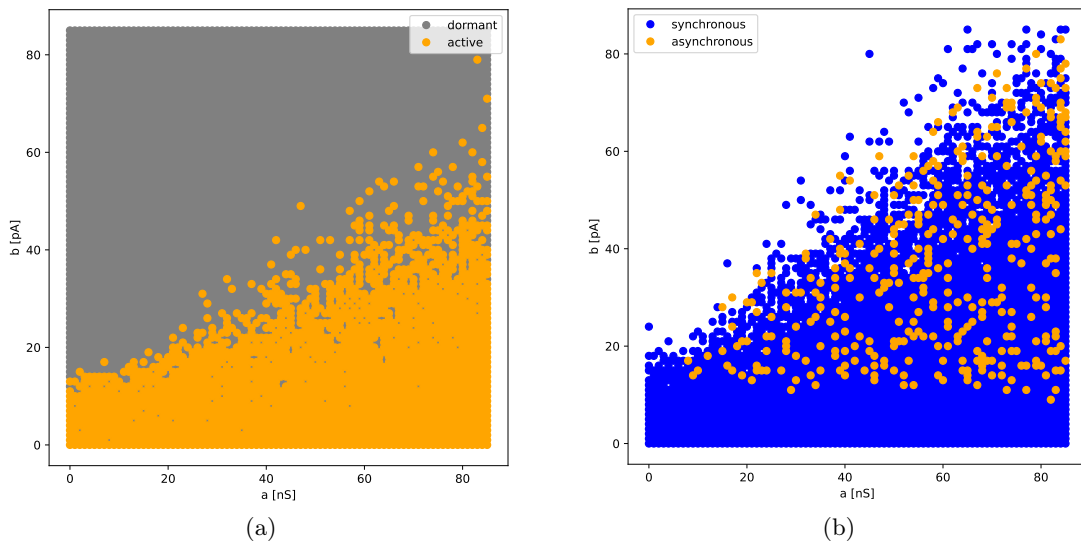


Figure 3: a) Conditions in adaptation space classified as dormant (grey) if 1 out of 3 replica did not show prolonged (after 1 s) activity, otherwise the network activity is classified as active (orange); b) adaptation space classified as a-/synchronous (mean coefficient of variation and pairwise correlation of replica satisfies asynchronous/irregular criteria)

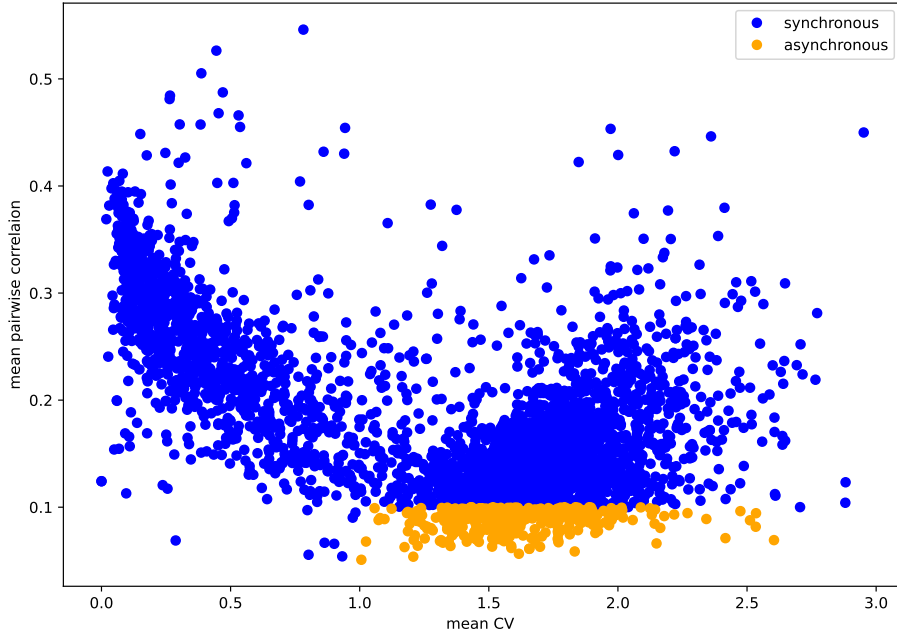


Figure 4: Active network conditions for adaptation space to measures of synchrony and regularity of network activity. Shows a bimodal distribution and highlights asynchronous states. CV stands for Coefficient of Variation.

$a$ [ $nS$ ]	$b$ [ $pA$ ]	$\bar{f}_r$ [ $Hz$ ]	$\sigma_{\bar{f}_r}$	$\bar{c}_v$	$\sigma_{\bar{c}_v}$	$\bar{\rho}_r$	$\sigma_{\bar{\rho}_r}$
<b>28</b>	<b>21</b>	28	8	1.5	0.5	0.081	0.007
84	65	29	1	1.4	0.1	0.073	0.005

Table 2: Top two favourite adaptation conditions ranked by highest coefficient of variation and correlation with their standard errors. All conditions for  $(g_e, g_i) = (40, 80) nS$ , Condition in bold was selected as the most asynchronous. Errors quoted according to Hughes, Ifan G., Hase [2010]

A ranking of conditions for highest coefficient of variation and correlation yields the two favorite conditions, listed in Table 2. We choose  $(a, b) = (28 nS, 21 pA)$  as the typical asynchronous, irregular network activity condition, as it lies within the region of average high coefficient of variation see Figure 5a.

On the other extreme, that is synchronous and regular network activity, we also choose the adaptation pair  $(a, b) = (5 nS, 14 pA)$ , i.e. lying in that strongly separate lower band in Figure 5.

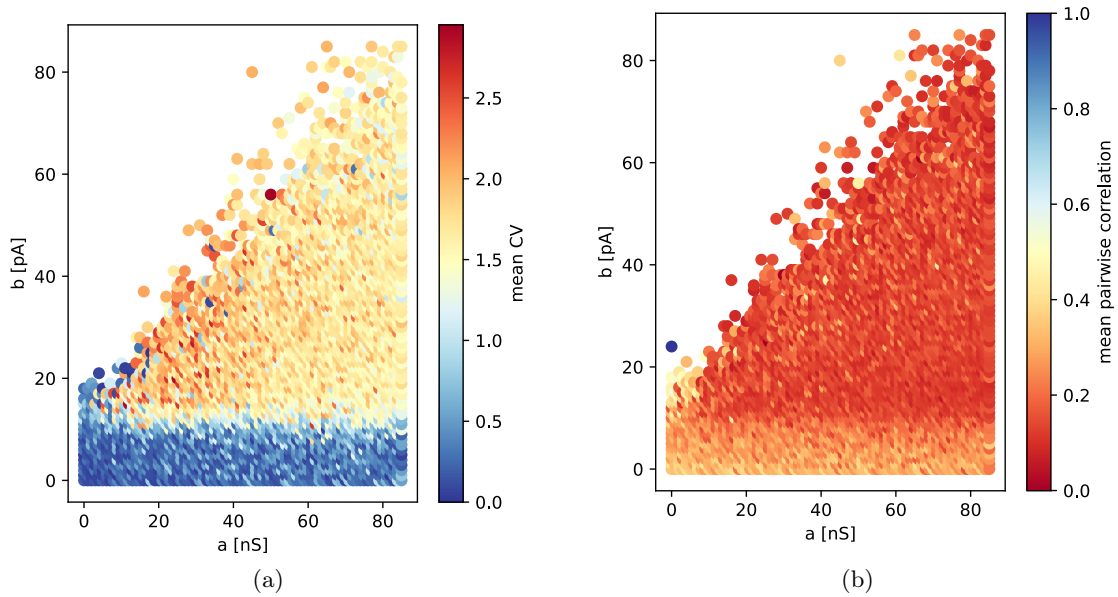


Figure 5: Heat-maps of both axis of network activity synchrony, regularity, i.e replica mean pairwise correlation a) and mean coefficient of variation b) respectively, over the adaptation space.

### 2.1.3 Extrema example network activities

To illustrate the actual difference in spiking pattern and how it relates to the values of coefficient of variation and correlation of the individual spike trains an example for each extreme of network activity is provided.

The network activity statistic are provided in Table 3. Note that the statistics and plots presented are for a single simulation / single network - these are not averaged activities from replicas as always before.

Figure 6 show an asynchronous and irregular network activity. Figure 7 show an synchronous and regular network activity. Note that both simulations do show a higher mean firing rate for inhibitory neuron as expected and physiologically sensible Susin and Destexhe [2021]

	$a$ [nS]	$b$ [pA]	$\bar{f}_r$ [Hz]	$\bar{c}_v$	$\bar{\rho}_r$
asynchronous, irregular	28	21	42	1.5	0.081
synchronous, regular	5	14	15	1.5	0.328

Table 3: Activity Statistics of example simulations. No standard errors calculated as these are statistics from single simulation, nevertheless. Quoted to precision as in Table 2

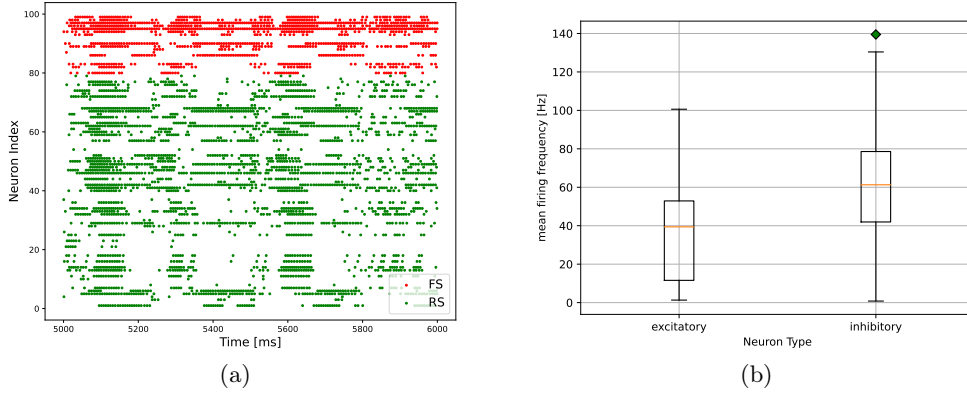


Figure 6: a) Raster plot and b) mean firing frequency of  $(a, b) = (28 \text{ nS}, 21 \text{ pA})$  and  $(g_e, g_i) = (40, 80) \text{ nS}$  as a prime example of a highly asynchronous and irregular network activity. FS indicates fast-firing inhibitory and RS regular firing excitatory neurons.

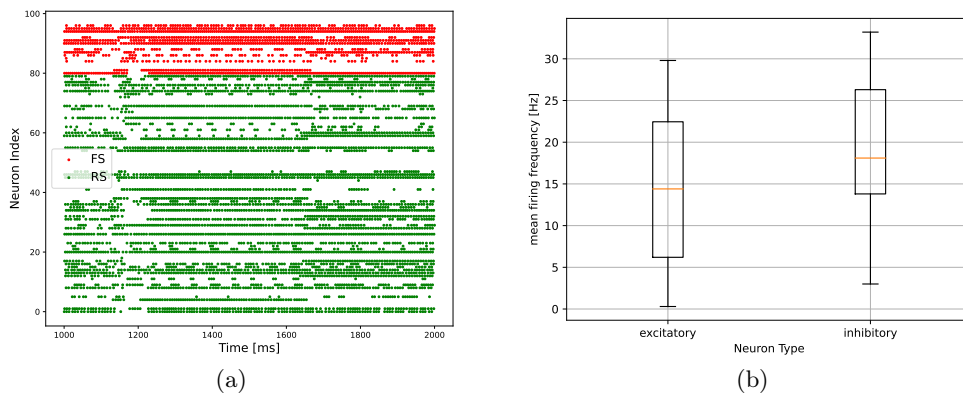


Figure 7: a) Raster plot and b) mean firing frequency of  $(a, b) = (5 \text{ nS}, 14 \text{ pA})$  and  $(g_e, g_i) = (40, 80) \text{ nS}$  as a prime example of a highly synchronous and regular network activity. FS indicates fast-firing inhibitory and RS regular firing excitatory neurons.

### 3 Impact of Synchrony on Functional Connectivity Inference

This section tries to answer the question to what extent synchrony and regularity of network activity influences functional connectivity inference with the cross-correlation algorithm by English et al. [2017].

For sake of illustration, this is not only done in a quantitative manner, i.e. inspecting the average inference performance, but also qualitatively for two extreme cases, showcasing the core working of the cross-correlation algorithm.

For all simulations presented in the following these demands were made: networks remain active beyond 9900 ms of simulation time; at least 15 active neurons. Further, note that the parameters of  $(g_e, g_i, a, b)$  of the extrema of synchrony identified in the prior section do not guaranty synchronous or asynchronous activity, just increase their relative frequency of occurrence. Hence, as we here do require guaranteed synchronous or asynchronous activity for the respective  $(g_e, g_i, a, b)$ -condition, i.e. simulation that do not satisfy are discarded. This statistically unproblematic, as only the network activity matters for the evaluation of performance of the connectivity inference.

The list of parameters used for the functional connectivity inference as defined by English et al. [2017] are listed in Table A1.

#### Synchrony Extrema Performance - Qualitative

In the following, the functional connectivity as been inferred for two examples networks.

Their spiking activity can be seen in Figure 8, and assures of the two extrema of synchrony and regularity.

Their network activity statistics are shown in Table 4 and show the demanded coefficient of variation and correlation. Note however that synchronous simulation have been found to consistently show high mean firing rates, yet far below the saturation frequency.

The connectivity inference algorithms performance for both cases can be seen in Figure 9 in the form of receiver operating characteristic (ROC). The asynchronous, irregular network activity in this case lead to a distinctly better performance with an area under the ROC curve of  $AUC = 0.744$ , compared to the synchronous case with a  $AUC = 0.588$ .

To illustrate to core working of the cross-correlation method for connectivity inference by English et al. [2017], selected correlogram are shown in Figure 10. See the figure caption for details.

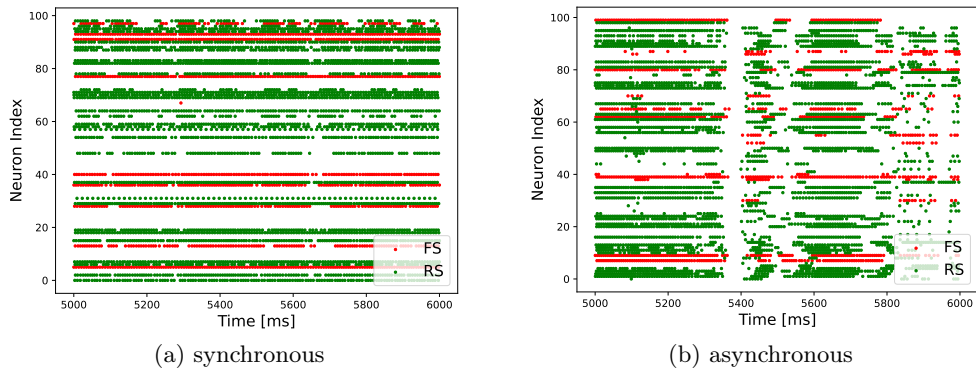


Figure 8: Raster plot of network activity of example simulations at the extrema of synchrony, regularity. FS indicates fast-firing inhibitory and RS regular firing excitatory neurons.

	synchronous	asynchronous
$f$ [Hz]	101	48
$\bar{c}_v$	0.5	1.8
$\bar{\rho}$	0.130	0.090

Table 4: Activity statistics of example simulations. No standard errors calculated as these are statistics from single simulation, nevertheless. Quoted to precision as in Table 2.

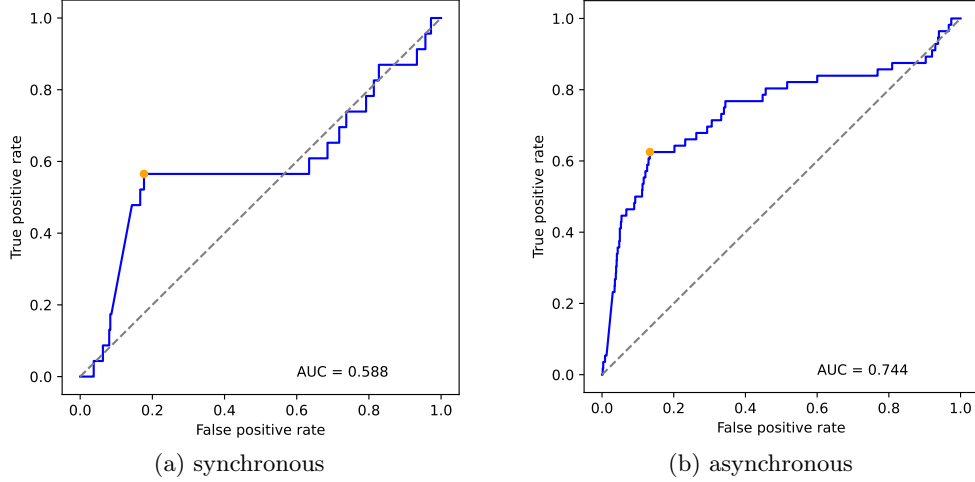


Figure 9: Receiver Operating Curves of the functional connectivity inference performed for the two example simulations at the extrema of synchrony, regularity. The selected threshold, i.e. the one closest to the perfect classifier on the ROC, is marked with an orange dot.

The full results of the connectivity inference as well as the analysis of the network topology see Appendix A. The inferred and true graphs can be found there in Figures A1 and A2. Note all graph representation in this report were drawn using the Kamada-Kawai path-length cost-function for positioning nodes. The threshold chosen for these particular inferred graphs was the threshold closest to the 'perfect classifier' (i.e.  $(TP,FP)=(1,0)$ ) on the ROC curve. For a better understanding of the network topologies, degree distributions, undirected/in/out, are shown in Figures A3 and A4.

For completeness all computed correlogram for are shown in Figure A5.

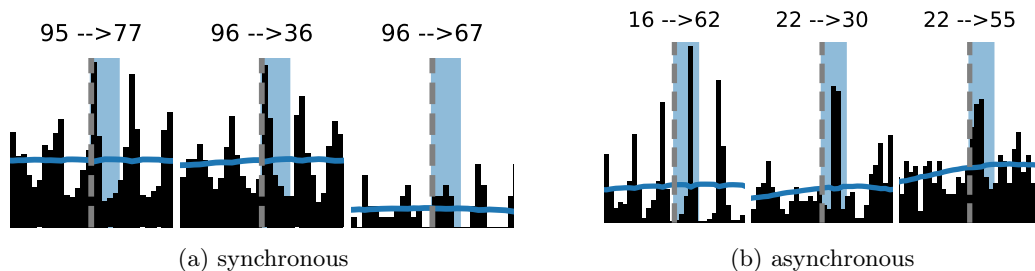


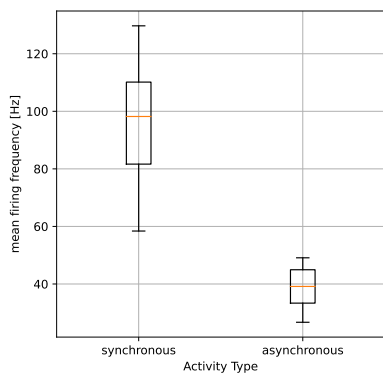
Figure 10: Each three examples of crosscorrelograms (CCG) computed in the functional connectivity inference performed for the two example simulations at the extrema of synchrony, regularity. Asynchronous CCGs show high counts in the synchrony window. Labels at the top indicate the neuron indices, i.e. indicating the directed edge or synapse evaluated. The vertical dashed grey line indicated the relative time-point,  $t = 0$ , of a spike in the pre-synaptic neuron. The black bar crosscorrelograms counts indicate the frequency of spiking at the relative time-point in the post-synaptic neuron. The blue line is a the frequency baseline rate,  $\lambda_{slow}$ , generated by the convolution of a hollow gaussian kernel ( $h_f = 0.6$ ) and the CCG counts with a standard deviation of  $10ms$  for smoothing. The blue vertical window is the synchrony window. Counts above the frequency baseline rate indicate a probable synapse between these two neurons. See English et al. [2017] for details on the method.

### Synchrony Extrema Performance - Quantitative

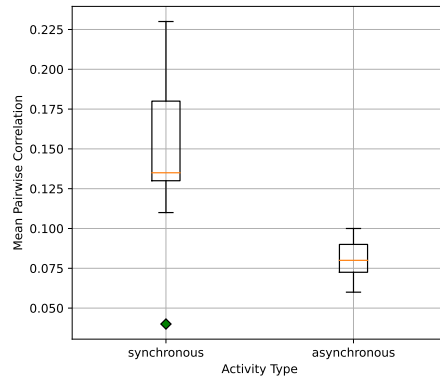
For the quantitative evaluation of the performance of the connectivity inference method 12 in-silico networks were simulated for each condition: a-/synchronous. This small number of 24 simulations were already sufficient to draw a conclusion for this project.

The network activity characteristics for the simulation are summarized in Figure 11. A clear difference between a- and synchronous activities is seen in the mean pairwise correlation and mean coefficient of variation - as demanded by definition. Noteworthy, is the difference in mean firing frequency. The synchronous network activities do result in much higher mean firing rates, which is probably due to the low value of the spike-triggered-adaptation,  $b$ , selected for synchronous simulations.

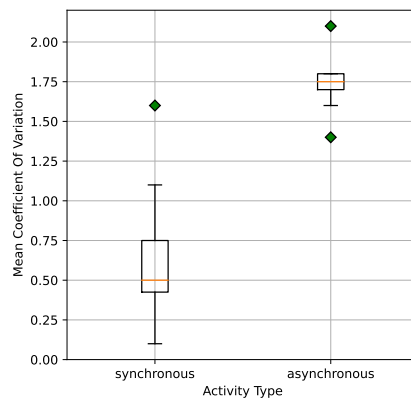
The summary of the connectivity inference ROC: Area Under the Curve is shown in Figure 12, as the main result of this study. A Welch's test yields a p-value of  $p = 0.9$ . There us no significant difference between the means of the two distributions. This study fails to discover a difference is performance of the functional connectivity inference method by English et al. [2017] between a- and synchronous network activities on small-scale networks. A significant difference was expected, especially with regard to network bursting often observed in-vitro neural recordings.



(a) Mean firing frequency



(b) Mean pairwise correlation



(c) Mean coefficient of variation

Figure 11: Box-plots for network activity characteristics for each 12 simulations for both extrema of synchrony, regularity of network activity.

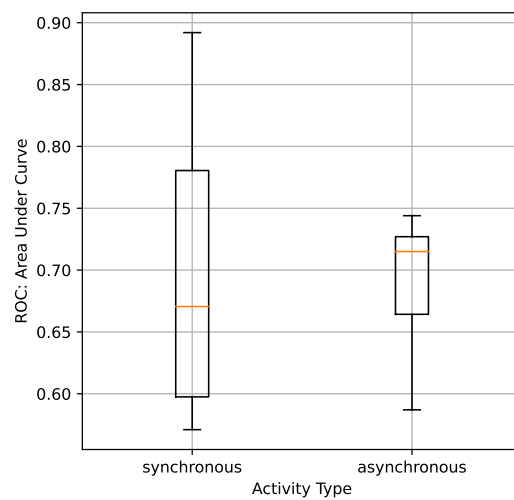


Figure 12: Box-plot of Area Under the Curve of the Receiver Operating Curves of both extrema of synchrony, regularity of network activity.

## 4 Impact of Topology

Another crucial consideration for the performance of connectivity inference methods in the neuronal network context must be the network topology. Different topologies cause different network activities.

Neuroscience literature currently favours the network topologies: Small-World topologies and Scale-Free networks. [Shimono and Beggs, 2014, Perotti et al., 2006, Shin and Kim, 2006]

The *small-world topology* is 'characterized by dense local clustering or cliquishness of connections between neighboring nodes yet a short path length between any (distant) pair of nodes due to the existence of relatively few long-range connections.' [Bassett and Bullmore, 2006] Biologically such a resource saving topology is enticing.

The *scale-free topology* has a power-law connectivity distribution, and their topology and evolution are governed by mechanisms such as preferential attachment and growth and is hence biologically enticing.

A topology that is both small-world and scale-free is hence biologically sensible, according to Shin and Kim [2006].

As part of this study first advances were made to implement different topologies, to then simulate neuronal network on top and analyze their network activity. Example simulation are shown here to showcase the functionality of the software written.

As the networks simulated here are all rather small (hence arguably small-world) we did choose to explicitly implement a method to generate scale-free networks. The working hypothesis is that a scale-free network with excitatory neurons at hubs with high out-degree should result in very synchronous firing.

### 4.1 Scale-Free Networks

More formally scale-free networks are defined to have a node degree distribution,  $P(k)$ , defined by a power law:

$$P(k) \propto k^{-\gamma} \quad (3)$$

where  $k$  is the node degree and  $\gamma$  the topology defining parameter.

As neuronal networks are directed graphs a further distinction between in- and out-degree arises. Thus a network is classified separately as scale-free for in-/out- or undirected degree.

The specific algorithm chosen to generate directed scale-free graphs originates from Bollobás et al.. The algorithm has three main topology defining parameters. Each is a probability of adding an edge and/or nodes. The algorithm grows a network by adding more nodes/edges based on those three probabilities. The parameters are:

- $\alpha$  probability for adding a new node connected to an existing node chosen randomly
- $\beta$  probability for adding an edge between two existing nodes chosen randomly
- $\gamma$  probability for adding a new node connected to an existing node chosen randomly

Further, parameters of the model are the in- and out-degree bias. All the following graphs are generated with an in-degree bias of  $\delta_{in} = 0.2$  and no out-degree bias.

In the following, the term "scale-rich" shall be used as opposed to scale-free as a further distinction from the random graph in the style of Li et al. [2005], yet not strictly applying the proposed metric.

## 4.2 Proof-of-Concept Simulations

Here three graphs were generated with the algorithm from Bollobás et al.. It was chosen to vary the  $\beta$  parameter at the cost of  $\alpha$  and  $\gamma$  to equal proportions. This results in three graphs of we shall refer to as scale-rich, intermediate and scale-free with increasing  $\beta$ . The parameters are shown in Table 5, accompanied by common network topology metrics.

	random	scale-rich	intermediate	scale-free
$\alpha$	-	0.35	0.25	0.1
$\beta$	-	0.2	0.5	0.8
$\gamma$	-	0.35	0.25	0.1
edges; edge density	200; 0.02	134; 0.013	168; 0.017	434; 0.04
mean node degree	3.86	2.68	3.36	8.68
mean clustering coefficient	0.03	0.04	0.11	0.27

Table 5: Graph generation parameters as defined by Bollobás et al. and other characteristics.

The three graphs are shown with a random graph, as generated by Gilbert [1959], for comparison in Figure 13. The corresponding degree distributions with gaussian and exponential fits are shown in Figure 14. The variation of the  $\beta$  parameter has clearly lead to more higher degree nodes with increasing  $\beta$ .

Raster plots of the three example neuronal network simulation run on top of those network topologies are shown in Figure 15. The corresponding network activity are shown in Table 6. Being single simulation values, no conclusions shall be drawn on their basis, yet the analysis has been put here to emphasize the kind of investigation that could be done in further works.

	random	scale-rich	intermediate	scale-free
mean firing frequency [Hz]	85.252	109.7	120.9	133.7
mean coefficient of variation	0.14	0.21	0.22	0.31
mean pairwise correlation	0.96	0.2	0.2	0.1

Table 6: Network activity characteristics; values of individual runs, put here do demonstrate the analysis - high variation for each

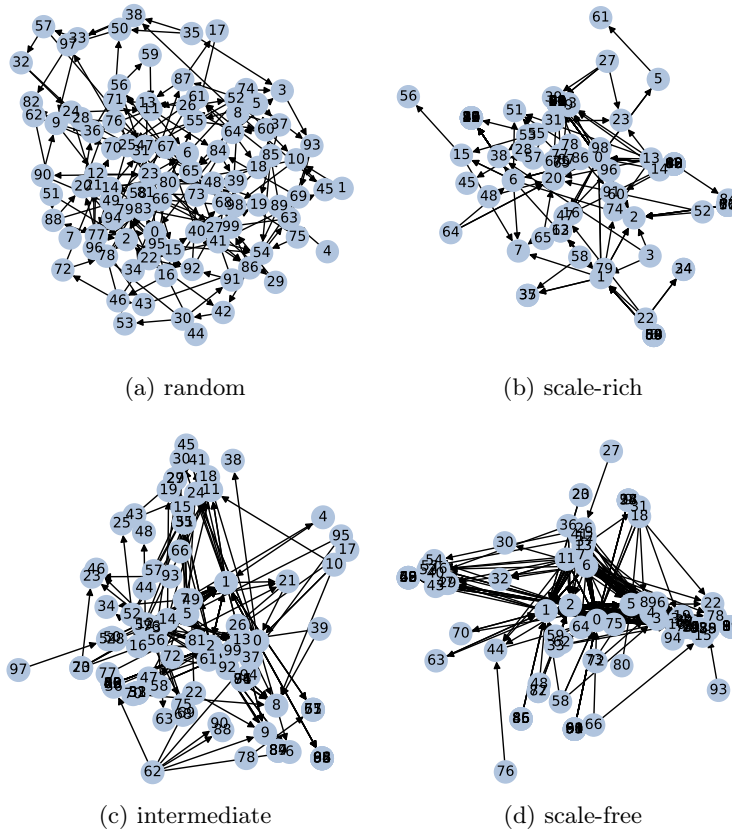


Figure 13: Graphs of the example simulations: a) random b) scale-rich, c) intermediate scale-free and d) most scale-free. Drawn using the Kamada-Kawai path-length cost-function for positioning nodes. See parameters in Table 5.

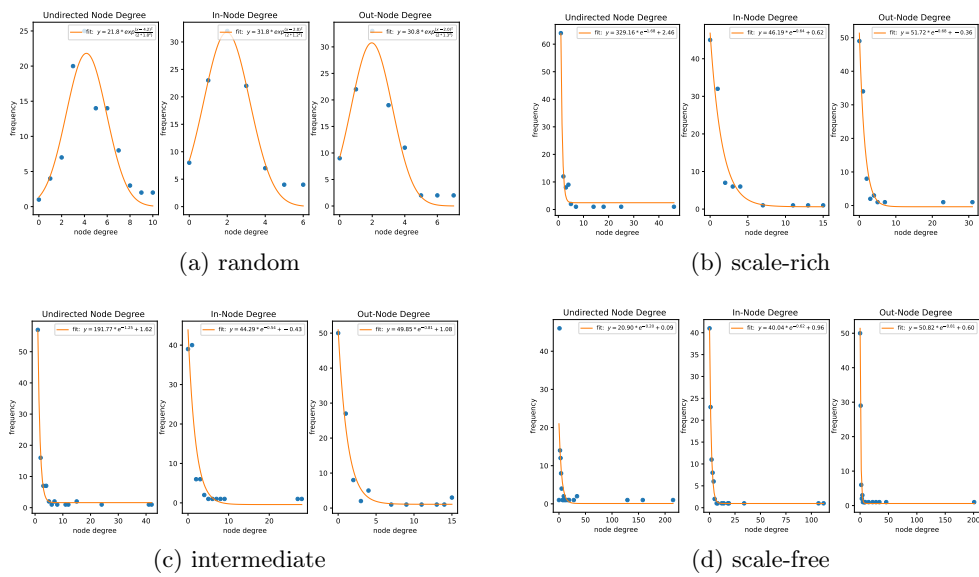


Figure 14: Networks degree distributions of the example networks generated with the respective fits (gaussian/exponential).

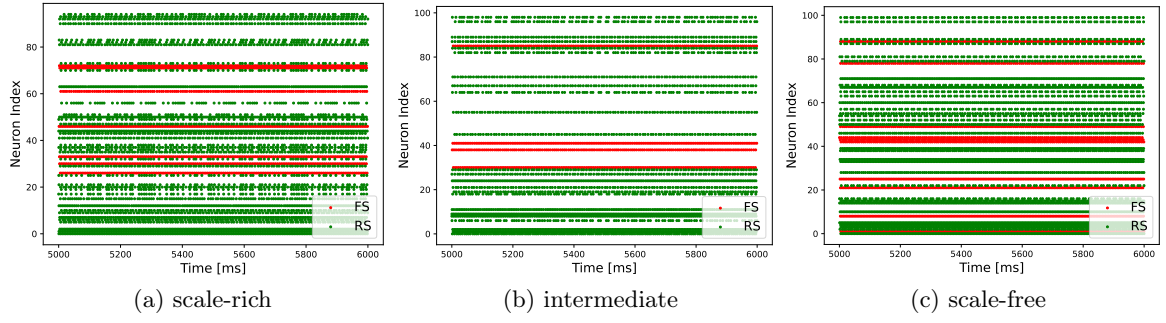


Figure 15: Raster-plots of network activity

### 4.3 Inhibitory Neurons as Hub Neurons

As a further step to realistic network topologies, the function to assign inhibitory neurons to nodes of high out-degree was implemented, as thought to be the case in neuronal network. Gal et al. [2021] No simulations of such kind are shown here as this feature leads to altering the total inhibitory current applied to the network in the current implementation - i.e. varying more than one property of the simulation at once. With slight modification this feature allows to study the role of inhibitory neurons as hub neurons.

## 5 Discussion & Conclusion

In this project a complete pipeline from generating and analyzing graph topologies, simulating neuronal networks and inferring their functional connectivity has been built. The neuron model implemented was closely based on Susin and Destexhe [2021] "Asynchronous and Irregular (AI) Network" implementation of the adaptive-Exponential Integrate-and-Fire (aEIF) by Brette et al. [2007]. As the main aim of this study the performance of the functional connectivity inference algorithm via cross-correlation by English et al. [2017] was evaluated. Due to resource constraints, this study focused on small-scale neuronal networks. In an extensive parametric study of the conductance and adaptation space of the aEIF model regimes of a-/synchronous and ir-/regular firing activity could be identified. The inference algorithm was thence evaluated at the found extrema of network activity. No significant difference in the performance of the inference was detected between the two cases, with respect to the ground truth graphs generated. As no 'bursting' networks were observed, it is likely that the small network size and the pre-selection of the "Asynchronous and Irregular (AI) Network" parameters by Susin and Destexhe [2021] already predisposed all our networks to be more asynchronous and irregular, leaving little difference between the two extrema compared in this study. Future studies should try larger networks evaluating a larger parametric space - both limited here by resources.

The parametric study conducted provides valuable insights and intuition of the workings of the aEIF model, as a side product.

The latter part of this study suggests further advances towards implementing more neurophysiological network topologies. As a showcase, example network activities of scale-free neuronal networks are shown with appropriate metrics, as guidance of future works.

For the systematic advancement in computational neuroscience, benchmarks of functional connectivity inference are needed to make novel findings comparable. This research project attempted this and shows some of the complexity of this task.

### Acknowledgements

The author of this paper would like to thank the following people for their contribution to this project:

<i>TaeHoon Kim</i> (ETH Zürich)	for his caring supervision of the project,
<i>Christian Donner</i> (Swiss Data Science Center)	for providing his implementation of the connectivity inference algorithm,
<i>Bioengineering Laboratory</i> (ETH Zürich)	for the means to conduct this highly computational study.

### Declaration of Work

A research project submitted in partial fulfilment of the requirements for the degree of Master of Biotechnology and the Diploma of Eidgenössische Technische Hochschule Zürich

All work presented here is my own work, is not copied from any other person's work (published or unpublished) unless otherwise indicated.

Visualization in this report were created using the matplotlib python libraries. All neuronal simulations were conducted using the Brian2 neuronal simulator.

Computations for this project were conducted on the Bioengineering Laboratory computing facilities of ETH Zürich.

## References

- D. S. Bassett and E. Bullmore. Small-World Brain Networks. *The Neuroscientist*, 12(6):512–523, dec 2006. ISSN 1073-8584. doi: 10.1177/1073858406293182. URL <http://journals.sagepub.com/doi/10.1177/1073858406293182>.
- B. Bollobás, C. Borgs, J. Chayes, and O. Riordan. Directed Scale-Free Graphs.
- R. Brette, M. Rudolph, T. Carnevale, M. Hines, D. Beeman, J. M. Bower, M. Diesmann, A. Morrison, P. H. Goodman, F. C. Harris, M. Zirpe, T. Natschläger, D. Pecevski, B. Ermentrout, M. Djurfeldt, A. Lansner, O. Rochel, T. Vieville, E. Muller, A. P. Davison, S. El Boustani, and A. Destexhe. Simulation of networks of spiking neurons: A review of tools and strategies, jul 2007. ISSN 09295313. URL <https://link.springer.com/article/10.1007/s10827-007-0038-6>.
- A. Destexhe. Self-sustained asynchronous irregular states and Up-Down states in thalamic, cortical and thalamocortical networks of nonlinear integrate-and-fire neurons. *Journal of Computational Neuroscience*, 27(3):493–506, dec 2009. ISSN 09295313. doi: 10.1007/s10827-009-0164-4. URL <http://link.springer.com/10.1007/s10827-009-0164-4><http://www.ncbi.nlm.nih.gov/pubmed/19499317>.
- D. F. English, S. McKenzie, T. Evans, K. Kim, E. Yoon, and G. Buzsáki. Pyramidal Cell-Interneuron Circuit Architecture and Dynamics in Hippocampal Networks. *Neuron*, 96(2):505–520.e7, oct 2017. ISSN 1097-4199. doi: 10.1016/j.neuron.2017.09.033. URL <http://www.cell.com/article/S0896627317309029/fulltext><http://www.cell.com/article/S0896627317309029/abstract>[https://www.cell.com/neuron/abstract/S0896-6273\(17\)30902-9](https://www.cell.com/neuron/abstract/S0896-6273(17)30902-9)<https://linkinghub.elsevier.com/retrieve/pii/S0896627317309029><http://www.ncbi.nlm.nih.gov/pubmed/29011111>.
- E. P. Frady and F. T. Sommer. Robust computation with rhythmic spike patterns. *Proceedings of the National Academy of Sciences of the United States of America*, 116(36):18050–18059, sep 2019. ISSN 10916490. doi: 10.1073/PNAS.1902653116/-/DCSUPPLEMENTAL. URL <https://www.pnas.org/content/116/36/18050><https://www.pnas.org/content/116/36/18050.abstract>.
- E. Gal, O. Amsalem, A. Schindel, M. London, F. Schürmann, H. Markram, and I. Segev. The Role of Hub Neurons in Modulating Cortical Dynamics. *Frontiers in Neural Circuits*, 15:96, sep 2021. ISSN 16625110. doi: 10.3389/FNCIR.2021.718270/BIBTEX.
- E. N. Gilbert. Random Graphs. *Source: The Annals of Mathematical Statistics*, 30(4): 1141–1144, 1959.
- J. S. Goldman, L. Kusch, B. Hazal Yalçınkaya, T.-A. E. Nghiem, V. Jirsa, and A. Destexhe. A comprehensive neural simulation of slow-wave 1 sleep and highly responsive wakefulness dynamics 2. *bioRxiv*, page 2021.08.31.458365, sep 2021. doi: 10.1101/2021.08.31.458365. URL <https://www.biorxiv.org/content/10.1101/2021.08.31.458365v1><https://www.biorxiv.org/content/10.1101/2021.08.31.458365v1.abstract><https://doi.org/10.1101/2021.08.31.458365>.
- A. L. Hodgkin and A. F. Huxley. A quantitative description of membrane current and its application to conduction and excitation in nerve. *The Journal of Physiology*, 117(4):500, aug 1952. ISSN 14697793. doi: 10.1113/JPHYSIOL.1952.SP004764. URL <https://www.ncbi.nlm.nih.gov/pmc/articles/PMC1392413/>.
- T. P. Hughes, Ifan G., Hase. *Measurements and their Uncertainties: A practical guide to modern error analysis*. Oxford University Press, Oxford, 2010. ISBN 978-0-19-956632-7.

- S. Inawashiro, S. Miyake, and M. Ito. Spiking neuron models for regular-spiking, intrinsically bursting, and fast-spiking neurons. In *ICONIP 1999, 6th International Conference on Neural Information Processing - Proceedings*, volume 1, pages 32–36, 1999. ISBN 0780358716. doi: 10.1109/ICONIP.1999.843957. URL <https://ieeexplore.ieee.org/stamp/stamp.jsp?tp=&arnumber=843957><https://ieeexplore-ieee-org.uproxy.library.dc-uoit.ca/stamp/stamp.jsp?tp=&arnumber=6617923>.
- T. R. Insel, S. C. Landis, and F. S. Collins. The NIH BRAIN Initiative. *Science*, 340(6133):687–688, 2013. ISSN 10959203. doi: 10.1126/SCIENCE.1239276.
- L. Li, D. Alderson, R. Tanaka, J. C. Doyle, and W. Willinger. Towards a Theory of Scale-Free Graphs: Definition, Properties, and Implications (Extended Version). *Applied Sciences*, page 44, jan 2005. doi: 10.48550/arxiv.cond-mat/0501169. URL <https://arxiv.org/abs/cond-mat/0501169v2>.
- I. Magrans de Abril, J. Yoshimoto, and K. Doya. Connectivity inference from neural recording data: Challenges, mathematical bases and research directions. *Neural Networks*, 102:120–137, jun 2018. ISSN 0893-6080. doi: 10.1016/J.NEUNET.2018.02.016.
- C. L. Martin and M. Chun. The BRAIN Initiative: Building, Strengthening, and Sustaining. *Neuron*, 92(3):570–573, nov 2016. ISSN 0896-6273. doi: 10.1016/J.NEURON.2016.10.039.
- J. Müller, M. Ballini, P. Livi, Y. Chen, M. Radivojevic, A. Shadmani, V. Viswam, I. L. Jones, M. Fiscella, R. Diggelmann, A. Stettler, U. Frey, D. J. Bakkum, and A. Hierlemann. High-resolution CMOS MEA platform to study neurons at subcellular, cellular, and network levels. *Lab on a Chip*, 15(13):2767–2780, jun 2015. ISSN 14730189. doi: 10.1039/c5lc00133a. URL <https://pubs.rsc.org/en/content/articlehtml/2015/lc/c5lc00133a><https://pubs.rsc.org/en/content/articlelanding/2015/lc/c5lc00133a>.
- E. Musk. An integrated brain-machine interface platform with thousands of channels. *Journal of Medical Internet Research*, 21(10):e16194, oct 2019. ISSN 14388871. doi: 10.2196/16194. URL <https://www.jmir.org/2019/10/e16194>.
- J. I. Perotti, F. A. Tamarit, and S. A. Cannas. A scale-free neural network for modelling neurogenesis. *Physica A: Statistical Mechanics and its Applications*, 371(1):71–75, nov 2006. ISSN 03784371. doi: 10.1016/j.physa.2006.04.079.
- A. Peyrache, N. Dehghani, E. N. Eskandar, J. R. Madsen, W. S. Anderson, J. A. Donoghue, L. R. Hochberg, E. Halgren, S. S. Cash, and A. Destexhe. Spatiotemporal dynamics of neocortical excitation and inhibition during human sleep. *Proceedings of the National Academy of Sciences of the United States of America*, 109(5):1731–1736, jan 2012. ISSN 00278424. doi: 10.1073/PNAS.1109895109/SUPPL\_FILE/PNAS.201109895SI.PDF. URL <https://www.pnas.org/doi/abs/10.1073/pnas.1109895109>.
- M. Shimono and J. M. Beggs. Functional Clusters, Hubs, and Communities in the Cortical Microconnectome. 2014. doi: 10.1093/cercor/bhu252. URL <http://code.google.com/p/>.
- C. W. Shin and S. Kim. Self-organized criticality and scale-free properties in emergent functional neural networks. *Physical Review E - Statistical, Nonlinear, and Soft Matter Physics*, 74(4):045101, oct 2006. ISSN 15502376. doi: 10.1103/PhysRevE.74.045101. URL <https://link.aps.org/doi/10.1103/PhysRevE.74.045101>.

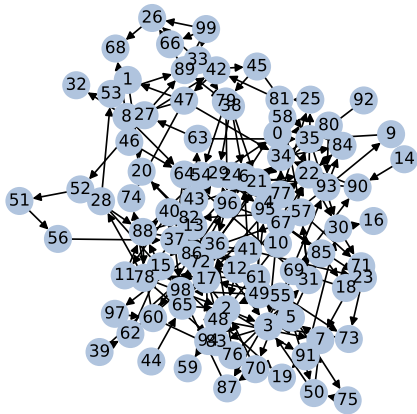
- E. Susin and A. Destexhe. Integration, coincidence detection and resonance in networks of spiking neurons expressing Gamma oscillations and asynchronous states. *PLoS Computational Biology*, 17(9):e1009416, sep 2021. ISSN 15537358. doi: 10.1371/journal.pcbi.1009416. URL <https://journals.plos.org/ploscompbiol/article?id=10.1371/journal.pcbi.1009416>.
- T. P. Vogels and L. F. Abbott. Signal Propagation and Logic Gating in Networks of Integrate-and-Fire Neurons. *Journal of Neuroscience*, 25(46):10786–10795, nov 2005. ISSN 0270-6474. doi: 10.1523/JNEUROSCI.3508-05.2005. URL <https://www.jneurosci.org/content/25/46/10786><https://www.jneurosci.org/content/25/46/10786.abstract>.
- J. Zhou, G. Cui, S. Hu, Z. Zhang, C. Yang, Z. Liu, L. Wang, C. Li, and M. Sun. Graph neural networks: A review of methods and applications. *AI Open*, 1:57–81, jan 2020. ISSN 26666510. doi: 10.1016/j.aiopen.2021.01.001.

# Appendices

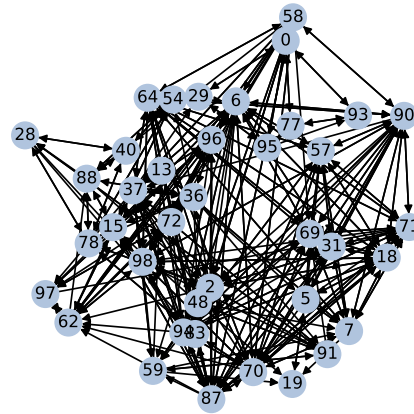
## Appendix A Full Results of Synchrony - Connectivity Inference

binsize [ $ms$ ]	1e-3
hollow fraction, $h_f$	.6
gaussian kernel standard deviation	0.01
synchrony window [ $ms$ ]	0, 5e-3
inspection window, $\tau_{CCG}$ [ $ms$ ]	20e-3

Table A1: Functional connectivity inference algorithm via cross-correlation parameters use as defined by English et al. [2017].

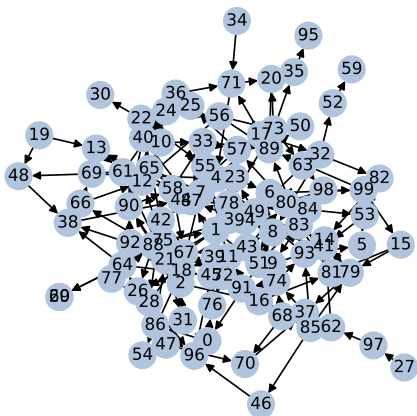


(a) true graph

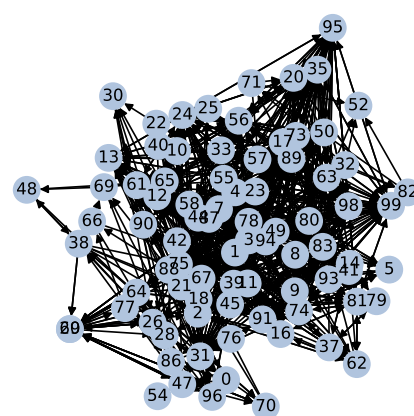


(b) inferred graph

Figure A1: Synchronous case



(a) true graph



(b) inferred graph

Figure A2: Asynchronous case

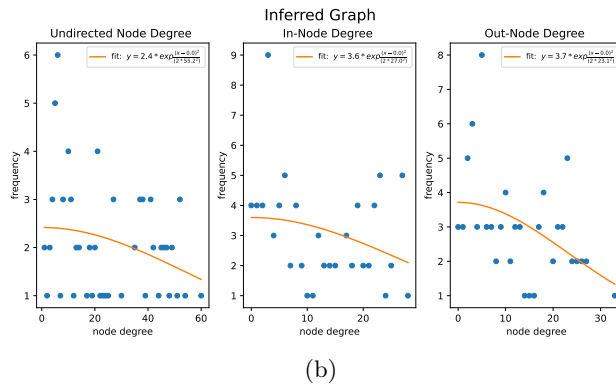
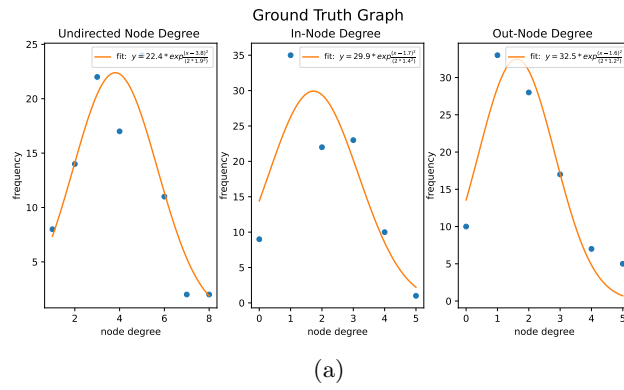


Figure A3: Synchronous Case

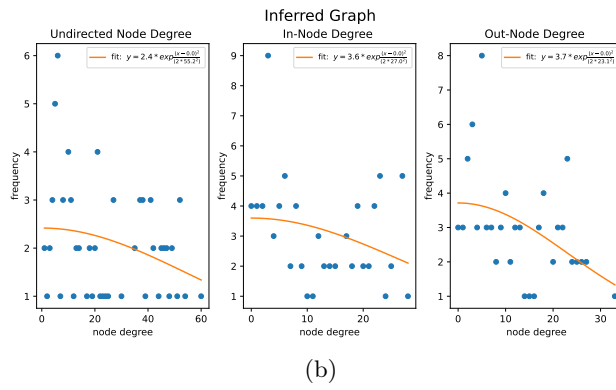
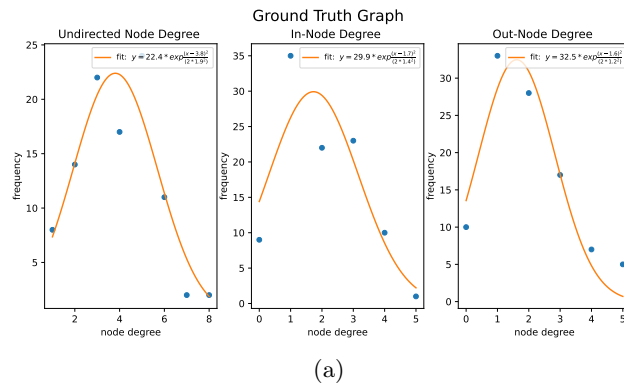
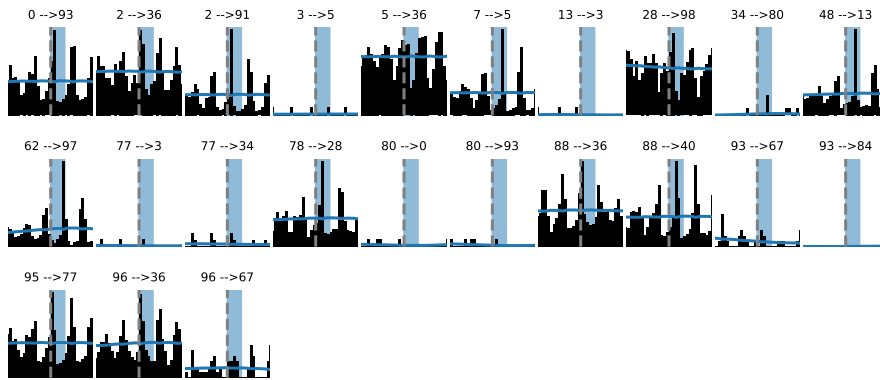
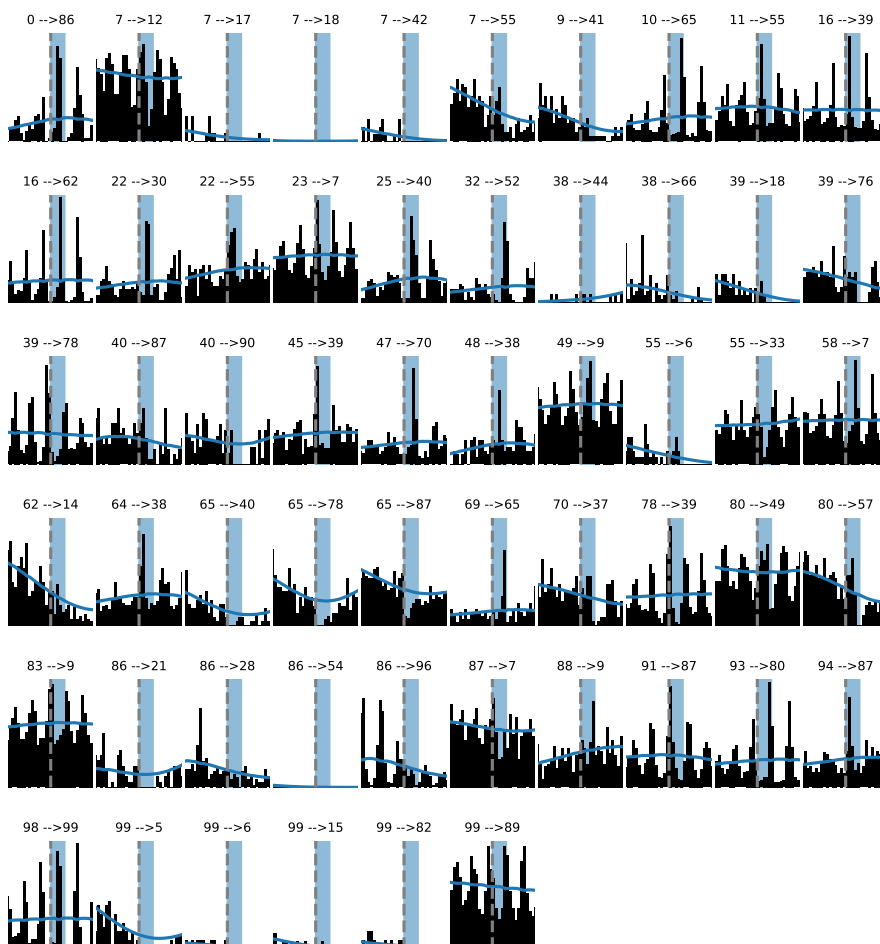


Figure A4: Asynchronous case



(a) Synchronous case



(b) Asynchronous case

Figure A5: All crosscorrelograms for both cases.

## Appendix B Source Code

The simulation and analysis code of this project can be found online:

<https://github.com/gordonkoehn/nexus>

The code allows for easy modification of network and model parameters and includes the code for the scale-free topology generation.

For further instructions of usage see the *README* in the repository or contact the author of this report.